

Thermal fields dynamics on a streamlined surface heated by a shock wave and a pulsed discharge

© I.A. Znamenskaya, E.A. Karnozova

Moscow State University, Moscow, Russia

e-mail: znamen@phys.msu.ru

Received February 22, 2024 Revised April 25, 2024 Accepted May 2, 2024

The thermal fields dynamics in the shock tube test chamber boundary layer on the wall surface close to a rectangular ledge was studied using the thermographic method. The heating and cooling of the wall behind the shock wave reflected from the ledge, as well as pulse discharge localization zone in the flow separation region, was studied. The wall heat registration in the range of $1.5\text{--}5.1\ \mu\text{m}$ was through the test chamber windows, transparent both for the wall thermal radiation and for the visible radiation of the discharge. It is shown, that in the channel surface in the shock-heated (for hundreds of microseconds) upwind zone, cooling occurs in a few milliseconds. The downwind zone, heated by a localized pulse discharge, wall cooling follows in a submillisecond time

Keywords: Shock tube, Separation zone, Infrared thermography, Heat fluxes, Localized sliding discharge.

DOI: 10.61011/TP.2024.06.58820.45-24

Introduction

Determination of convection and thermal conductivity heating of channel walls in a boundary layer of a high speed flow both has a fundamental value related to studying the processes of high speed gas dynamics and physical and chemical kinetics [1], and an applied value related to determination of the properties of heat protective materials, ensuring optimal conditions for streamlining the surfaces, and also combustion in the combustion chambers of aircraft [2,3]. When such processes are modeled, it is possible to implement and monitor quite a wide range of flow parameters in shock pipes of various types [4,5]. Heating of the streamlined surface may be caused by shock wave impact and impact of gas dynamic flow, and also plasma impact of various duration — when discharges of various type are initiated. However, the time of the operating mode in such units is limited. For local measurements of heat flux in impulse gas dynamic and plasma dynamic processes, various special sensors are used [1,4]. To determine the spatiotemporal characteristics of dynamic thermal fields, thermal imaging devices were used [5]: the method of panoramic thermographic visualization of nonstationary thermal fields was used to register them on the end wall of the rectangular channel in the shock pipe. The obtained thermograms of the outer side of the channel end wall give an idea on distribution of the heat emission intensity for various moments of time after shock pipe reflection. Measurements for the incident shock wave with Mach number $M = 1.5$ demonstrate that the emission intensity varies for different areas of the investigated section of the shock pipe — zone of the flux core and near the boundaries of the end ledge.

High speed thermography is used to study nonstationary processes happening in air tunnels as well [6]. Using a high speed infrared thermograph, temperature oscillations were

recorded on a heated thin foil. High spatial (around 2 mm) and temporal (around 100 Hz) resolutions enable measurement of spatiotemporal distribution of heat fluxes in an air tunnel. Thermographic studies of heat fluxes are carried out in the mode of stationary streamlining of obstacles as well; in [7] a cylinder streamlining thermogram was obtained, made via side windows that are transparent for infrared radiation in the supersonic stationary flow with Mach number $M = 3$ after establishment of the thermodynamic equilibrium.

Infrared thermography is used for contactless recording of widely differing thermal processes [8]; in particular, important results were obtained when studying interaction of jets of fuel and air mixtures with the walls in engine studies [9]. Analysis of thermal imaging images obtained from the foil side opposite to the injection zone, demonstrated efficiency of spray cooling as the wall temperature increases.

Registration of thermal field dynamics is used as one of the methods to diagnose processes happening in the plasma devices [10,11]. Measurements of the temperature on the side surface of the outer electrode of the plasma accelerator were carried out 5 ms after the discharge with the help of a thermal imager in the spectral range of $3.7\text{--}4.8\ \mu\text{m}$ and integration time of 1 ms at frame rate of 200 Hz [11]. It is shown that thermography of the electrode side surface makes it possible to determine the position of the discharge in the accelerator. Heating of the dielectric surface developed by plasma actuators is studied by various methods, including infrared thermography [12]. It is shown that thermography may provide information on the spatial and temporal distribution of dielectric temperature. Attempts have been made to establish a connection between distribution of temperature of the dielectric surface and gas temperature [13]. Various observations demonstrate that the dominant mechanism of heat transfer from plasma to dielectric happens through convection from a hot air flow.

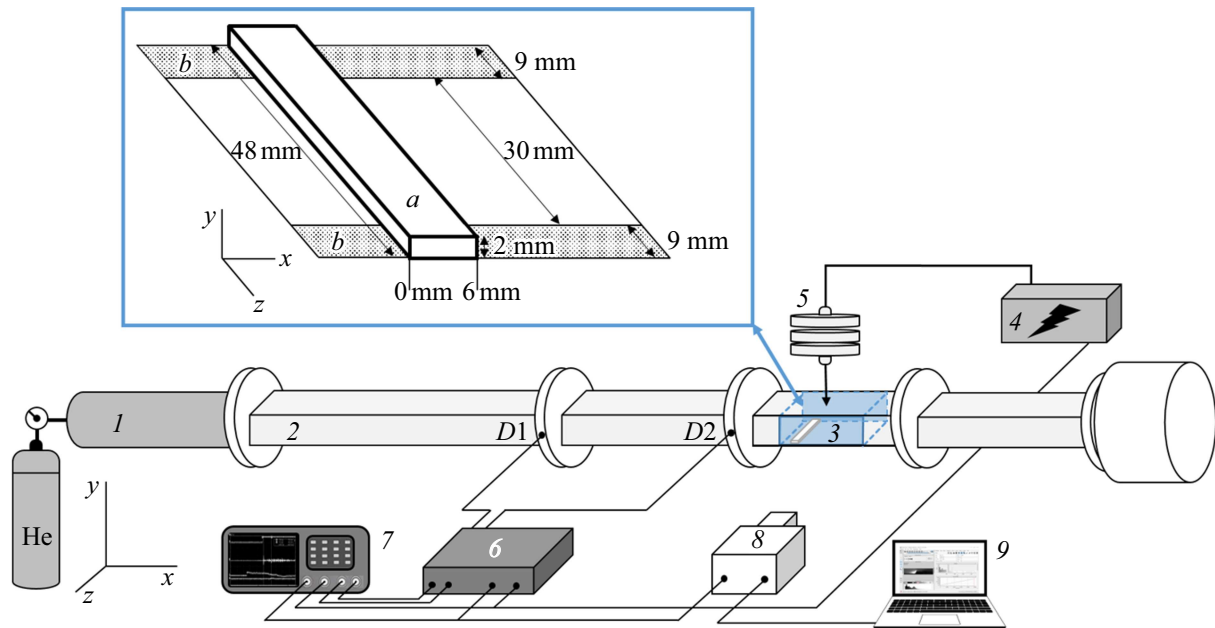


Figure 1. Experimental bench circuit diagram: 1 — high pressure chamber filled with helium, 2 — low pressure chamber filled with air, 3 — discharge section built into low pressure chamber: *a* — dielectric ledge, *b* — copper electrodes, 4 — discharge initiation block with high voltage source, 5 — capacitor, 6 — synchronization system, 7 — oscilloscope, 8 — thermal imager, 9 — thermogram processing software complex. *D1*, *D2* — piezoelectric transducers built into a shock pipe channel.

As dielectric barrier discharge (DBD) ignites in the absence of the outer flow [14], measurements show quick and substantial increase of dielectric temperature, of the order of 50°C. Quick dielectric temperature drop is observed in the outer approach flow; the conducted temperature measurements show that the turbulent boundary layer above the discharge provides for substantially better heat removal compared to the laminar one.

High speed gas flow control includes shock wave impact at the flow, change of heat fluxes on the streamlined surfaces, energy supply. At the same time the boundary layer liftoff areas, laminar-turbulent transition, jump positions, etc. are monitored. In the general case the mechanisms of impact from impulse (submicrosecond) near-surface energy supply to the flow based on the electric discharge are different in different time scales. In the problems of flow control with the help of impulse discharge plasma the quick gas heating is of outstanding interest — in the nanosecond time scale. When the impulse discharge current flows, simultaneously there is direct impact of a short-lived plasma formation on the gas dynamic flow and surface (submicrosecond range) [15]. Then in the microsecond time range the surface heating is implemented by shock-wave, gas dynamic processes, caused by impulse energy contribution in the flow; then the surface heated with plasma and flow cools down.

The objective of this paper is panoramic research of thermal fields evolution and benchmarking of spatiotemporal characteristics of areas related to gas dynamic and plasma mechanisms for heating of the sections in the wall of the

gas dynamic channel with a rectangular ledge, based on the method of high speed infrared thermography.

1. Experimental setup

Experiments were carried out on UTRO-3 bench (Shock Pipe-Discharge-Optics) (Fig. 1). In the channel of the low pressure chamber of 2 single-membrane shock pipe of rectangular cross section 48×24 mm there is a special discharge section built in 3 with the same cross section and side walls of 15 mm thickness made of quartz glass. On the upper and lower walls of the discharge chamber at the distance of 24 mm from each other there are two high current discharges that were initiated and slide on the dielectric surface (plasma sheets) [16]. A plasma sheet was initiated between a pair of copper electrodes with length of 100 mm and thickness of 0.1 mm, located aflush on the dielectric wall. The area of the plasma sheet was 100×30 mm. The voltage impulse initiates the development of the distributed sliding discharge with duration of 100–200 ns. The impulse surface discharge in the homogeneous flow had a multi-channel structure: it represented a set of parallel plasma microchannels across the flow with length of 30 mm, distributed along the dielectric surface with length of 100 mm. When a discharge is initiated in the heterogeneous boundary layer, the discharge is mainly localized in the area with low density, in particular, in the flow liftoff areas [15]. To research the evolution of thermal fields 1) — in heterogeneous nonstationary gas dynamic flow and 2) — in the flow with localized impulse energy

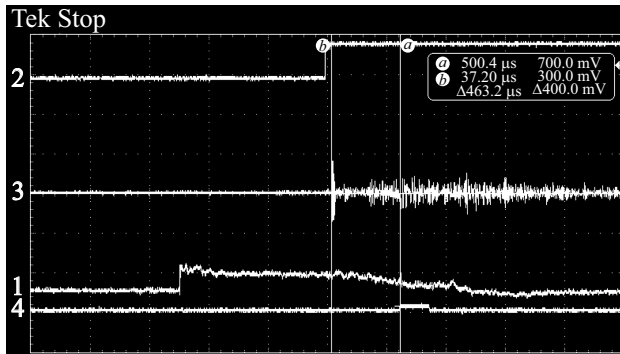


Figure 2. Signals registered by oscilloscope. Horizontal scale: $400 \mu\text{s}$ in a cage, 1 — signal from sensor D1 (SW pass), 2 — signal of infrared camera initiation, 3 — signal from sensor D2 (SW pass), 4 — signal recording the moment of impulse discharge initiation, *a*, *b* — cursors making it possible to define the time intervals of interest.

supply, a dielectric ledge was installed on the lower wall of the channel in the form of a parallelepiped. It had the size of $48 \times 6 \times 2 \text{ mm}$ and was located between two windows at the distance of 20 mm from the start of the lower plasma electrode area. Thermographic studies of thermal fields were carried out on the lower wall of the channel (with the ledge). The discharge was connected via a capacitor 5, charged to voltage $\sim 25 \text{ kV}$, via an initiation block 4. Discharge current oscillograms were registered with the help of a special shunt (with band width 1 GHz).

Signals from piezoelectric transducers (D1 and D2 in Fig. 1), installed in the shock pipe channel, signal of thermal imaging recorder start and signal of discharge current are recorded by oscilloscope Tektronix TPS 7. Data obtained from the oscilloscope (Fig. 2) make it possible to calculate edge speed and Mach number (M) of the shock wave (SW) in the channel; to determine the moment of thermal imaging camera start, the moment of discharge initiation. This enables calculation of the time interval between the moment of SW passing the front edge of the dielectric ledge ($t = 0$) and the moment of discharge initiation — delay time (t_p). Since during the experiments the duration of the thermal imager frame exposure (from 0.2 to 1.0 ms) is much higher than the specific times of the researched high-rate gas dynamic processes ($1\text{--}2 \mu\text{s}$), it is necessary that the researched time interval of the gas dynamic heating (and cooling down) process got in the interval of the thermal imaging survey exposure. Start of the shooting with the camera relative to the start of the discharge from the external signal was adjusted by the synchronization system (δ in Fig. 1).

Research of thermal fields inside the discharge section channel (registration of the thermal emission from the lower surface of the channel) was carried out via side windows using an infrared (IR) camera (thermal imager) Telops FAST M200. Spectral range of camera: $1.5\text{--}5.1 \mu\text{m}$, camera speed — $\leq 2080 \text{ Hz}$, frame exposure duration — $\leq 0.2 \text{ ms}$. Quartz

windows of the camera have high infrared transmittance in the operating range of the thermal imager. Registration in all experiments was carried out at angle 87° from the normal line to the lower surface of the wall. Due to design features of the bench, it was not possible to increase the observation angle. Comparison of thermal fields in all thermal imaging frames was carried out with account of the following: 1) — emission coefficient at angles $60\text{--}90^\circ$ from the normal line to the recorded surface is hardly dependent on the material (metal, dielectric) [17]; 2) — the shooting angle did not change in the experiments. Digital cameras Nikon D50 and Canon EOS 500D recorded in the visible range the integral images of discharge plasma glow.

2. Results and discussion

Thermographic survey visualized thermal fields formed on the lower wall of the channel after interaction of flat SW with Mach number $M = 2.8\text{--}3.3$ with the rectangular ledge (obstacle). Parameters of gas (homogeneous flow) downstream the flat SW are determined from Rankine-Hugoniot relations using known parameters of the environment upstream the SW edge and SW speed (Mach number). Then in the flow the subsequent procedure for movement of breaks and disturbances in the area of the bench working camera may vary — upon implementation of various initial conditions (preferably upon variation of pressures in high and low pressure chambers) [18]. Change of the gas temperature downstream the shock wave edge and in the downstream flow causes the relevant change in time of heat fluxes on the streamlined surfaces, heating of the inner surfaces of the channel: upper and lower walls of the working camera, three walls of the obstacle, side walls. In the first hundreds of microseconds after passage of the shock wave with the used values of Mach number via the obstacle - cocurrent flow-supersonic one, upstream the ledge-obstacle in the channel a reflected shock wave appears (braking wave), which with time travels further along the flow. For the same time (less than 1 ms) the hot gas downstream the receding SW heats the sections in the flat upper wall, lower wall with the ledge, and also inner surfaces of two side walls of the discharge section [19]. Then the approach cocurrent flow stops being supersonic, the obstacle streamlining pattern changes. After the cold depression wave reflected from the high pressure chamber arrives (in 1-3 ms), the walls are cooled down.

Studies of the thermal fields in the lower walls near the rectangular ledge were performed — from windward and lee sides. The obtained consistent thermograms reflect the dynamics of heating and cooling of these areas. Thus, if SW passes with Mach number $M = 3.0 \pm 0.2$, air temperature upstream its edge was 297 K, temperature beyond the SW edge — around 800 K. After the SW passes by the dielectric ledge, an impulse surface charge was initiated in the downstream flow with different delay in the discharge section channel. Thermal emission from areas heated

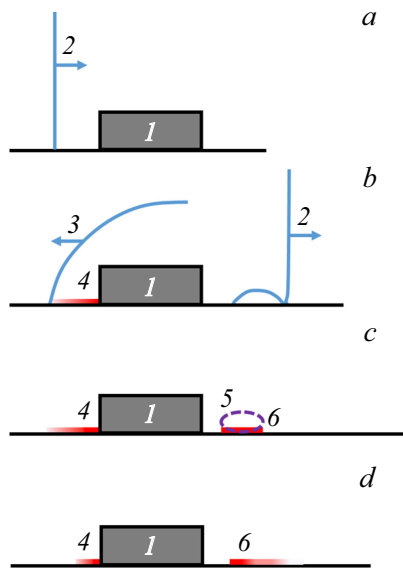


Figure 3. Circuit diagram of channel lower wall heating: 1 — ledge, 2 — incident SW, 3 — reflected SW, 4 — heating area in windward zone, 5 — discharge plasma localization area, 6 — heating area in lee zone (after the discharge).

bu short-lived plasma formation, was also recorded by a thermal imager.

As the surface discharge is initiated in the supersonic flow, two main mechanisms are implemented for heating of the lower channel wall (the circuit diagram is shown in Fig. 3). Thermal processes include 1) — interaction of approach and reflected SW in the windward area with the lower wall (Fig. 3, *a, b*) and 2) — interaction of discharge plasma and initiated disturbances with the lower wall in the lee area — downstream the obstacle (Fig. 3, *c, d*).

Thermal imaging images including the discharge plasma glow do not record the thermal emission of plasma [3]. Time scales more specific for thermal processes and survey data using an IR camera in the experiment (millisecond range), considerably exceed the nanomicrosecond impulse processes upon discharge initiation. Therefore, one frame of thermal imaging shooting is an integral image reflecting not only radiation of nanosecond plasma formation, and the fixing data of thermal fields recorded in the absence of plasma, i.e. at subsequent moments of time (within the exposure time). The synchronization system enables monitoring the time of registration start. As a result on the second and subsequent thermograms the main source of thermal emission are the sections of dielectric surfaces in the interelectrode area, which cool down after the end of the impulse heating (discharge plasma in the first frame is distant from each of the side walls by 8–9 mm — electrode width).

The time of delay between the moment of flat SW passing the windward wall of the obstacle and the moment of impulse surface discharge initiation varied within $t_p = 0.06–1.00$ ms. In this time interval the flow speed is

quite high (more than 700–800 m/s). With time the speed of cocurrent flow downstream the passed SW reduces, the flow creates turbulence. Selection of delay time makes it possible to initiate discharge at various stages of flow development.

Discharge redistribution occurs in accordance with the change of the flow pattern as the flow streamlines the dielectric obstacle [15]. Various stages of flow evolution correspond to various modes of discharge localization near the obstacle. After shock wave diffraction, a liftoff area is formed beyond the backward facing step (lower density area). When the impulse surface discharge is initiated in such flow in the section of the lower wall with the ledge, the discharge plasma is localized in the lee liftoff area (lower density area) in the form of a short-lived high current plasma channel [15].

The surface discharge initiated in this flow mode is visualized as a short-lived plasma formation, being a transverse plasma channel with length of around 30 mm, parallel to the side wall of the obstacle (Fig. 4). In the lee area beyond the backward facing step a submicrosecond energy contribution is implemented in the discharge localization area [15]. As a result, the short-term heating of the corresponding section in the lower wall of the channel takes place.

Thermographic registration of thermal fields was completed on the walls of the channel in the working chamber of the shock wave under simultaneous thermal impact of the impulse localized near-surface plasma area and shock-wave heating of the surfaces after non-stationary interaction of SW with the obstacle. Spatiotemporal parameters of thermal fields on the lower wall were compared, which are caused by plasma heating and the boundary layer in the flow downstream the flat and reflected SW.

Fig. 5 shows subsequent images of thermal fields in the lower wall of the channel after passage of the flat SW with Mach number $M = 2.8$ (Fig. 5, *a, b*), upon initiation of the surface discharge (Fig. 5, *c*) and subsequent evolution of thermal fields in this section (Fig. 5, *d–f*). The discharge is initiated after a time delay $t_p = 0.85$ ms, the ellipse means an area heated by discharge. Dashed lines show the boundaries of the lower wall with the obstacle. Horizontal dashed lines show the positions of the lower walls and side windows crossing lines. The following is reflected in the remote window: to the left from the ledge — hot area of windward wall of the obstacle in the flow braking area in



Figure 4. Integral shot of discharge plasma optical glow in flow downstream SW. Arrows indicate flow direction, dashed line — obstacle boundaries.

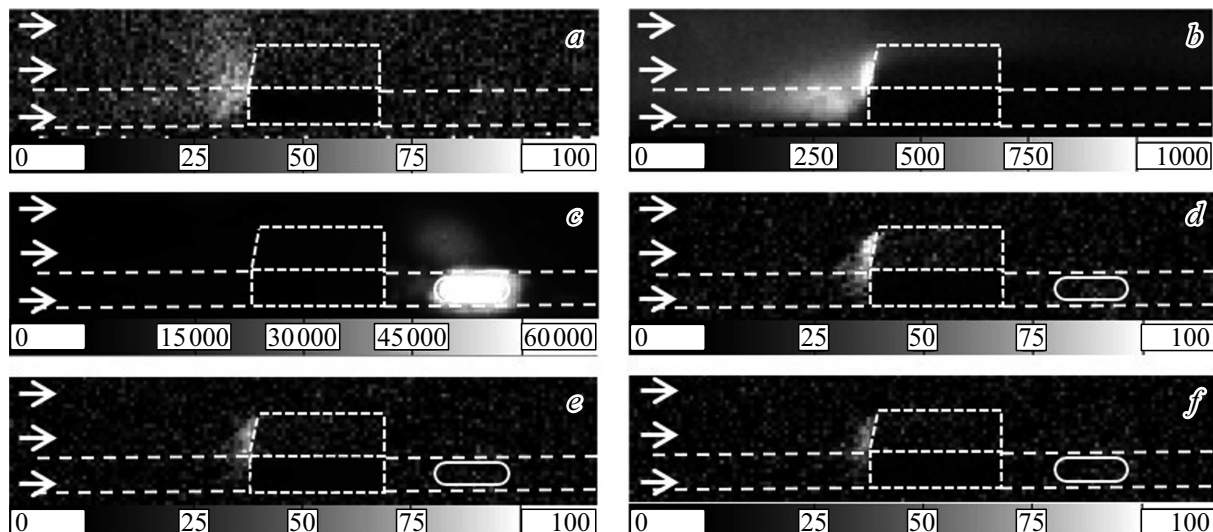


Figure 5. Subsequent thermal imaging images, camera speed 2080 Hz, time of single frame exposure 0.25 ms: *a, b* — gas dynamic heating of the wall in lee area, *c* — lower wall radiation from the discharge localization area, *d–f* — cooling down of heated areas in the flow.

Fig. 5, *a, b, d–f*) and to the right from the ledge — discharge plasma (Fig. 5, *c*).

Quantitative measurements of the thermal radiation were completed in one intensity scale in conventional units (a. u.) (Fig. 6). Change of the value range on the scales of images shown in Fig. 5, *b, c* depends on the change of the limit value of radiation on thermograms at various moments of time. Thus, in Fig. 5, *c* intensity of radiation from the section of the lower wall in the lee area (discharge plasma glow) substantially exceeds the intensity values in the windward area; in the selected intensity range caused by radiation of the discharge area, the windward area looks dark, despite the presence of the heat flux exceeding the background values.

Data obtained from a series of panoramic shots make it possible to track change of radiation intensity in the windward and lee areas near the obstacle with time. To analyze dynamics of thermal processes, temporal dependences were built for cooldown of areas locally heated by discharge plasma, and comparison was done to the data obtained from heating and cooldown of the channel sections in the flow without discharge initiation (Fig. 6). The curve presents the values of thermal radiation intensity from two corresponding sections of the shock wave channel lower wall surface depending on time after SW passage ($t = 0$) of the front wall of the ledge ($x = 0$ mm, (Fig. 1)).

The lines indicate average values recorded by a thermal imager for intensity of radiation of the lower wall upstream the ledge (frame exposure time $250 \mu\text{s}$). Averaging was done by the area of most intensive radiation of the lower wall recorded on the thermograms; the survey area had the length of 2 mm ($x = -2-0$ mm), covering the entire width of the lower wall (from glass to glass). The actual size of the selected section in the lower wall is 2×48 mm, on the

thermograms the size of the survey area was 2×2 mm, since the shooting was carried out at the angle to the lower wall surface. The vertical line on the curve indicates a moment of time of surface discharge initiation and its localization in the lee area (Fig. 3, *c*). Duration of the discharge current is around 150 ns, for this period of time the large portion of the discharge energy is released [20]. In the near surface lee area of the flow the heat exchange happens in the liftoff area. Due to short term contact of the plasma with the surface, no heat conductivity to the wall is implemented for this time interval, in contrast to the radiation-convection heat exchange. The points represent the average measured values of thermal radiation intensity in the lower wall in the lee area after discharge plasma initiation. Measurements were carried out in the registration area with length of 1.5 mm: $x = 12-13.5$ mm — in the area downstream the flow from the discharge localization area.

For the time of the first frame exposure ($t = 0.00-0.25$ ms) SW passes along the channel of the operating chamber of the shock wave; the boundary layer in the cocurrent flow heats the wall surfaces. Further in the windward area a reflected SW arises as a result of streamlining of the ledge with approach flow next to a straight step and interacts with all the channel walls upstream the ledge. It also heats the lower wall in the windward area, which you can see on the curve as intensity rise ($t = 0.0-0.8$ ms). Data presented in Fig. 6, means that the intensity of thermal radiation of the windward surface of the lower wall increases and reaches the maximum value in 0.5–0.8 ms. Besides, the maximum length of the gas dynamic heating zone of the lower wall increased from 2 mm (averaging area) to 5–6 mm in the upward flow direction ($x = 6-0$ mm). With time the reflected shock wave moves upstream and weakens. The lower wall of

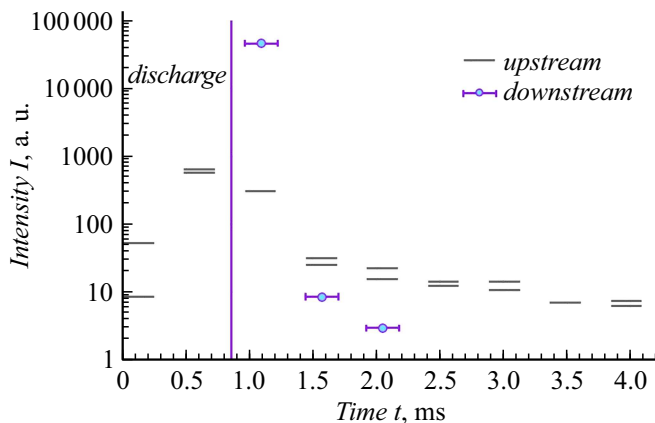


Figure 6. Time dependences of thermal radiation intensity in channel lower wall (in conventional units). SW Mach number $M = 2.8$.

the channel cools down in the approach flow, and thermal radiation intensity decreases. Thermal radiation relaxes for 3–4 ms as the cocurrent flow cools down after passage of the plug heated by the shock wave. The longest cooldown was observed near the windward wall of the straight step in the flow braking area.

At the specified moment of time ($t = 0.85$ ms) the surface discharge is initiated downstream the shock wave, which quickly heats the lower wall area in the impulse energy contribution localization area (in the liftoff area — lower density area). It is shown that there the heating of the surface to the maximum intensity happens for the time of around $100 \mu\text{s}$ after initiation of the discharge plasma. You can see that the intensity values in the area heated by energy contribution substantially exceed the values of the thermal radiation of gas dynamic heating in the windward wall. On the frame obtained after discharge initiation ($t = 0.95$ ms), one can observe the maximum intensity of radiation downstream the discharge channel area. Besides, the windward area has thermal radiation intensity that is much lower than that of the lee one. On the next frame in 0.5 ms in the lee area the measured heating by plasma discharge is already lower than in the windward area. Both intensities of thermal radiation exceeded the background values and made around 30 and 10 conventional units in the windward and lee areas, accordingly. The plasma localization area heated by the discharge cools down quickly: due to short-term heating of the surface, the wall heat conductivity mechanism is not implemented. By the moment of time $t = 1.5$ ms ($t = 0.65$ ms after the discharge) the thermal trace is nearly absent. It is shown that relaxation of the thermal radiation of the wall in the lee area of plasma localization takes place for less than 1 ms. Besides, it is noted that the end intensity of thermal radiation from the discharge localization area was lower than the end intensity in the windward area heated by gas downstream the reflected wave for a long period of time — before arrival of the cold area of the flow (expansion wave in the cocurrent

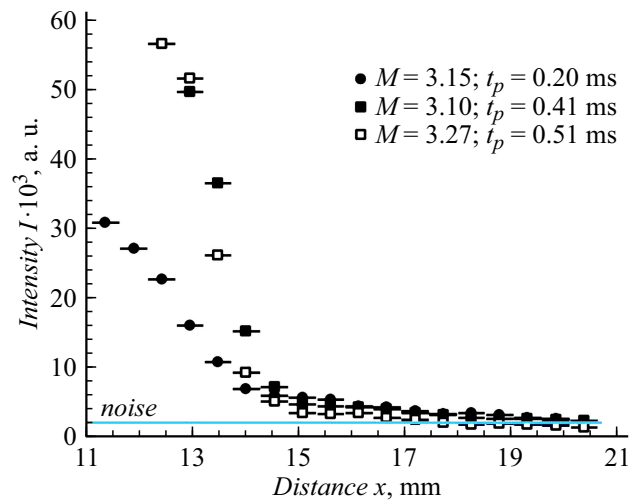


Figure 7. Distribution of intensity (in conventional units) of thermal radiation of the lower wall in lee area for various SW Mach numbers and delay times t_p .

flow formed by membrane rupture and reflected from the end of the high pressure chamber).

To analyze the area heated by discharge plasma, dependence was built between the lower wall radiation and distance along the flow direction (Fig. 7).

The curve shows the distribution of intensity of lower wall thermal radiation downstream the discharge plasma localization area. Time interval of every measurement is 0.5 ms — duration of frame exposure, the delay time between the moment of SW passage and the moment of discharge initiation t_p varied. Much numbers of the approach SW are $M = 3.10$ (black squares), $M = 3.15$ (points), $M = 3.27$ (white squares), the delay time increased from $t_p = 0.20 \pm 0.05$ ms (points), to $t_p = 0.41 \pm 0.05$ ms (black squares) and $t_p = 0.51 \pm 0.05$ ms (white squares). The growth of thermal radiation intensity (approximately double) is obviously related to the fact that the wall heating time could not fully get into the interval of time of the exposure (0.5 ms) as the discharge initiation was delayed after shock wave passage 0.20 ms, but was included only partially. If the delay increases 2–2.5 times, accordingly the time to register the actual impact of the discharge on the wall increases; the highest value of radiation intensity is observed as accumulated for the increased registration time. The distance x is counted from the windward wall of the obstacle (Fig. 1). Values were read from the plasma localization area (optical emission area) to the end of the area recorded on the frame, which corresponds to the distance 21.00 ± 0.25 mm. This area of optical emission varied for different delay times. It is shown that the intensity of the thermal emission is highest near the area of plasma localization and at longest time of delay (and registration) (11 mm for $M = 3.15$, $t_p = 0.20 \pm 0.05$ ms; 12 mm for $M = 3.27$, $t_p = 0.51 \pm 0.05$ ms; 13 mm for $M = 3.1$, $t_p = 0.41 - 0.05$ ms). At a distance from the

plasma localization area approximately at 17–19 mm from the windward wall of the ledge, the intensity drops substantially and reaches the noise level (horizontal line in Fig. 7). This is due to the fact that the discharge provides for short-term heating of the flow in the area of its localization, and the heat taken by the flow from the heated area has no time to heat the wall of the channel located downstream.

Conclusion

The dynamics of thermal fields was researched by thermographic method in the boundary layer on the streamlined surface of the wall of the gas dynamic channel (shock wave). To research the evolution of thermal fields in heterogeneous nonstationary gas dynamic flow and in the flow with localized nanosecond discharge, a dielectric ledge was installed on the lower wall of the channel in the form of a parallelepiped with size of $48 \times 6 \times 2$ mm. The ledge was located between the working chamber windows. The thermal imager registered nonstationary processes of channel wall heating and cooling down upstream and downstream the ledge after interaction of the flat SW with Mach number $M = 2.8$ – 3.3 with a rectangular step in the range of 1.5–5.1 m via the side windows of the working chamber with frame exposure 250–500 μ s. Spatiotemporal characteristics of thermal fields were compared: 1) in zones of heating and cooling down of the windward area downstream the shock wave reflected from the ledge and 2) in the flow downstream the ledge in the lee area in the impulse near surface discharge localization area.

The distribution of intensity of wall thermal radiation in the lee liftoff area downstream from the discharge plasma localization area was obtained. The dependence was built between intensity of thermal emission of the channel lower wall (in conventional units) and time for various delay times of discharge initiation in the nonstationary flow downstream the shock wave.

It is shown that in the shock-heated windward area of the channel lower wall (in the area of reflected SW escape and flow breaking upstream the ledge) the intensity of thermal fields radiation happens within hundreds of microseconds. Then in 3–4 ms the intensity drops (after arrival of the expansion wave). The maximum length of the gas dynamic heating of the lower wall upstream the ledge as recorded by the thermal imager is assessed as 5–6 mm.

Cooling down of the lee section of the channel wall downstream the ledge heated by impulses with the sliding nanosecond discharge localized to the liftoff area, happens for much shorter time — less than 1 ms; the heating zone length — up to 4 mm downstream.

Funding

This study was supported financially by grant No. 23-19-0096 from the Russian Science Foundation.

Conflict of interest

The authors declare that they have no conflict of interest.

References

- [1] M.A. Kotov, P.V. Kozlov, V.Yu. Levashov, G.Ya. Gerasimov, N.G. Solovyov, A.N. Shemyakin, M.Yu. Yakimov, V.N. Glebov, G.A. Dubrova, A.M. Malyutin. *Tech. Phys. Lett.*, **49**(9), 34 (2023). DOI: 10.61011/TPL.2023.09.56705.19633
- [2] M. Fenot, E. Dorignac. *Int. J. Therm. Sci.*, **109**, 386 (2016). DOI: 10.1016/j.ijthermalsci.2016.06.010
- [3] T. Ombrello, D.L. Blunck, M. Resor. *Exp. Fluids.*, **57**, 140 (2016). DOI: 10.1007/s00348-016-2210-0
- [4] Yu.V. Dobrov, V.A. Lashkov. *Tech. Phys.*, **67**(9), 1137 (2022). DOI: 10.21883/TP.2022.09.54676.39-22
- [5] I.A. Znamenskaya, M.I. Muratov. *Tech. Phys. Lett.*, **49**(8), 77 (2023). DOI: 10.61011/TPL.2023.08.56695.19643
- [6] H. Nakamura. *Spatio-Temporal Measurement of Convective Heat Transfer Using Infrared Thermography, Heat Transfer - Theoretical Analysis, Experimental Investigations and Industrial Systems*, ed. by Prof. Aziz Belmiloudi (National Defense Academy, Japan, 2011)
- [7] S.S. Popovich, N.A. Kisleev, A.G. Zditovets, Y.A. Vinogradov. *J. Phys.: Conf. Ser.*, **2039**, 01202 (2021). DOI: 10.1088/1742-6596/2039/1/012029
- [8] V.P. Vavilov. *Infrakrasnaya termografiya i teplovoy kontrol*, 2-e izd., dop. (Izdat. dom „Spektr“, M., 2013) (in Russian)
- [9] M. Zaccara, C. Carvallo, A. Montanaro, J. Gimeno, L. Allocca, G. Cardone. *Exp. Therm. Fluid Sci.*, **142**, 110825 (2023). DOI: 10.1016/j.expthermflusc.2022.110825
- [10] A.V. Voronin, V.Yu. Goryainov, V.K. Gusev. *Tech. Phys.*, **65**(6), 987 (2020). DOI: 10.1134/S1063784220060286
- [11] V.Yu. Goryainov, M.E. Viktorov, A.V. Vodop'yanov, A.V. Voronin. *Tech. Phys.*, **66**(2), 325 (2021). DOI: 10.1134/S1063784221020134
- [12] X. Zhang, Yu. Zhao, Ch. Yang. *Chinese J. Aeronaut.*, **36**(1), 1 (2023). DOI: 10.1016/j.cja.2022.01.026
- [13] R. Tirumala, N. Benard, E. Moreau, M. Fenot, G. Lalizel, E. Dorignac. *J. Phys. D: Appl. Phys.*, **47**, 255203 (2014). DOI: 10.1088/0022-3727/47/25/255203
- [14] R. Jousot, V. Boucinha, R. Weber-Rozenbaum, H. Rabat, A. Leroy-Chesneau, D. Hong. *40th Fluid Dynamics Conference and Exhibit* (Chicago, Illinois, USA, 2010), DOI: 10.2514/6.2010-5102
- [15] I. Znamenskaya, A. Lutsky, D. Tatarenkova, E. Karnozova, N. Sysoev. *Phys. Fluids*, **35**, 076110 (2023). DOI: 10.1063/5.0153624
- [16] I.A. Znamenskaya, D.F. Latfullin, I.V. Mursenkova. *DAN*, **427**(1), 32 (2009) (in Russian)
- [17] V.V. Korotaev, G.S. Melnikov, S.V. Mikheev, V.M. Samkov, Yu.I. Soldatov. *Osnovy teplovideniya* (NIU ITMO, SPb., 2012), p. 17 (in Russian).
- [18] D.I. Dolbnya. *kand. diss. (MGU im. M.V. Lomonosova, M., 2023)* (in Russian), <https://dissovet.msu.ru/dissertation/2580>
- [19] I.A. Znamenskaya, M.I. Muratov, E.A. Karnozova, A.E. Lutsky. *Sci. Vis.*, **15**(3), 92 (2023). DOI: 10.26583/sv.15.3.10
- [20] I.V. Mursenkova, A.Yu. Kuznetsov, A.S. Sazonov. *Appl. Phys. Lett.*, **115**, 114102 (2019). DOI: 10.1063/1.5116810

Translated by M. Verenikina